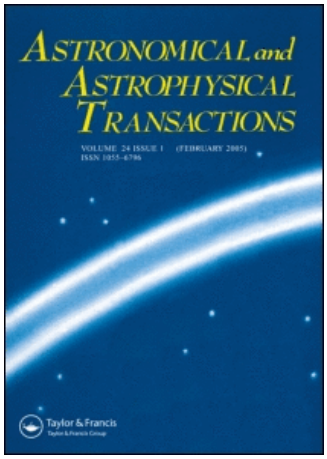

Astronomical & Astrophysical Transactions
The Journal of the Eurasian Astronomical Society
Publication details, including instructions for authors and subscription information:
http://www.informaworld.com/smpp/title~content=t713453505

Simulations of the dynamics of the lest

H. Jakobsson [a]
[a] Lund Observatory, Lund, Sweden

Online Publication Date: 01 July 1997
To cite this Article: Jakobsson, H. (1997) 'Simulations of the dynamics of the lest', Astronomical & Astrophysical Transactions, 13:1, 35 - 46
To link to this article: DOI: 10.1080/10556799708208113
URL: http://dx.doi.org/10.1080/10556799708208113

Astronomical and Astrophysical Transactions, 1997, Vol. 13, pp. 35–46
Reprints available directly from the publisher
Photocopying permitted by license only

SIMULATIONS OF THE DYNAMICS OF THE LEST

H. JAKOBSSON

Lund Observatory, Box 43, S-221 00 Lund, Sweden

(Received November 22, 1995)

A model of the dynamics of the Large Earth-based Solar Telescope (LEST) is briefly described. The model includes the various subsystems of the telescope, with emphasis on its live optics system, which is used to correct for various kinds of disturbances, in particular the atmospheric turbulence, in real time. The disturbances are also modelled, and used as input to the telescope model. The modelling of the atmospheric turbulence is described, and results from simulations show the influence of the atmosphere during different seeing conditions.

KEY WORDS Atmospheric effects, methods: numerical, telescopes, Sun: general

1 INTRODUCTION

Ground-based observations of the Sun are of fundamental importance within the field of solar physics. Many important phenomena on the Sun occur on comparatively small spatial scales and require telescopes with high angular resolution when observed from Earth. However, the resolution of existing solar telescopes is limited by several factors, in particular the atmospheric turbulence. Also, the relatively small apertures of the telescopes define a fundamental limit for the angular resolution that in principle can be reached. By today's standards, even the diffraction limit of existing solar telescopes is becoming a limiting factor.

In order to overcome the limits imposed by today's solar telescopes, a new solar telescope, the Large Earth-based Solar Telescope (LEST), is being planned. Since the construction of the telescope will inevitably be rather complex, a model of the telescope, with emphasis on the dynamics, has been implemented.

2 THE TELESCOPE

2.1 Optical Design

The design of the LEST is described in detail elsewhere (Engvold and Andersen, 1990). Here, only a brief description of the optical path of the light, as seen in Figure 1, will be given.

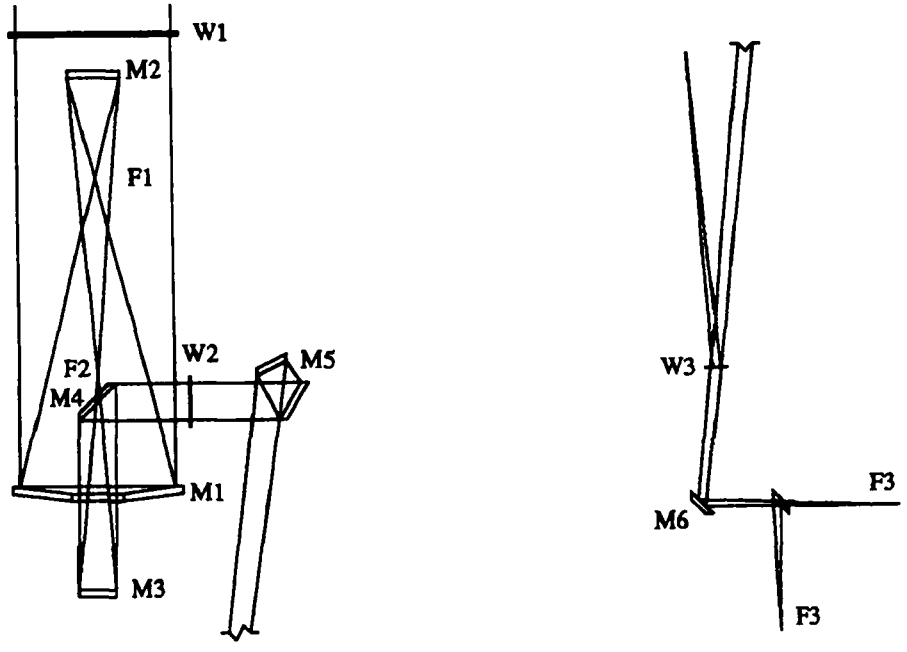

Figure 1 The optical layout of the LEST.

Propagating through the telescope to the final focus F3, the light first passes the entrance window W1, into the helium filled telescope tube. It is then reflected by the parabolic primary mirror M1, passes the primary focus F1, where a heat trap is located, is reflected by the elliptic secondary mirror M2, passes the secondary focus F2, where a polarization modulator may be placed, and is then reflected by the elliptic tertiary mirror M3. This mirror relays the image from F2 (and F1) to F3.

On its way from M3 to F3, the light is reflected by the flat mirror M4, leaves the helium filled telescope tube through the small window W2, and enters an evacuated tube, where it is reflected by the flat mirror M5 into an almost vertical direction. The light leaves the evacuated tube through the small window W3, and enters the air above the rotating instrument table. A small fraction of the light is reflected upwards from W3 to the slow wavefront sensor. A flat mirror M6 directs the light out over the instrument table, where some post-focus instrument is placed in the position F3. A seventh mirror may sometimes be used to direct the light downwards, to post-focus instruments in a vertical shaft.

The optical design of the LEST is such that one can identify two kinds of image motion in the final focus F3: motion of the limb of the field-of-view, here referred to as field-of-view tilt, and motion of the solar granulation pattern inside the field-of-view, here referred to as wavefront tilt. The latter is the image motion seen by the observer. All sources of image motion will result in wavefront tilt, but only those

located after the heat trap will cause field-of-view tilt, of an amount equal to the wavefront tilt caused by the same source.

2.2 The Live Optics System

The LEST will have an aperture diameter of 2.4 m, which is considerably larger than that of any existing solar telescope. High-resolution imaging is one of the main priorities of the LEST, and the telescope is designed to be able to obtain solar images of an unprecedented, essentially diffraction limited quality. In order to achieve such a high image quality, the telescope will be equipped with a live optics system, consisting of active optics, adaptive optics and systems for automatic alignment and autoguiding (Andersen *et al.*, 1993). In Figure 2, a somewhat simplified overview of the telescope and its live optics system is seen.

The active optics is used to compensate for low temporal frequency effects such as thermal and gravitational effects, imperfections of mirror surfaces etc. The compensations are performed by deformation of the primary mirror M1, except for focus adjustments, which are carried out by moving M3 along the optical axis. The adaptive optics compensates for high temporal frequency effects, caused by atmospheric turbulence and wind gusts. This is done by tilting and deforming M5, which, as seen in Figure 1, will be divided into two mirrors, one fast tip-tilt mirror and one deformable mirror.

The live optics system also includes a correlation tracker, a slow wavefront sensor, a solar limb guider, a field-of-view guider and various machanical servo systems. The correlation tracker performs two-dimensional correlation calculations on solar images, and is needed for the telescope to be able to keep pointing at a particular feature on the solar surface. The wavefront sensor senses the aberrations of the wavefronts, and the limb guider is used for tracking of the Sun. The field-of view guider, finally, is used to avoid excessive motion of the field of view while minimizing the wavefront filt.

As indicated in Figure 2, the active optics is dependent on signals from the slow wavefront sensor, and the adaptive optics on signals from the correlation tracker. Further, not shown in the figure, there is an independent system for low temporal frequency adjustments of the pressure inside the helium filled telescope tube. The pressure is kept equal to that of the air outside, in order to avoid optical effects (defocus, spherical aberration and polarization) introduced by bending of the entrance window W1.

3 THE TELESCOPE MODEL

As seen above, the telescope design is fairly complex. Therefore, in order to verify the functioning of the various interdependent subsystems and of the telescope as a whole, and to determine to what extent the telescope will be able to fulfill the requirements regarding image quality, a simulation of the dynamics of the entire telescope, with emphasis on the live optics system, is in progress.

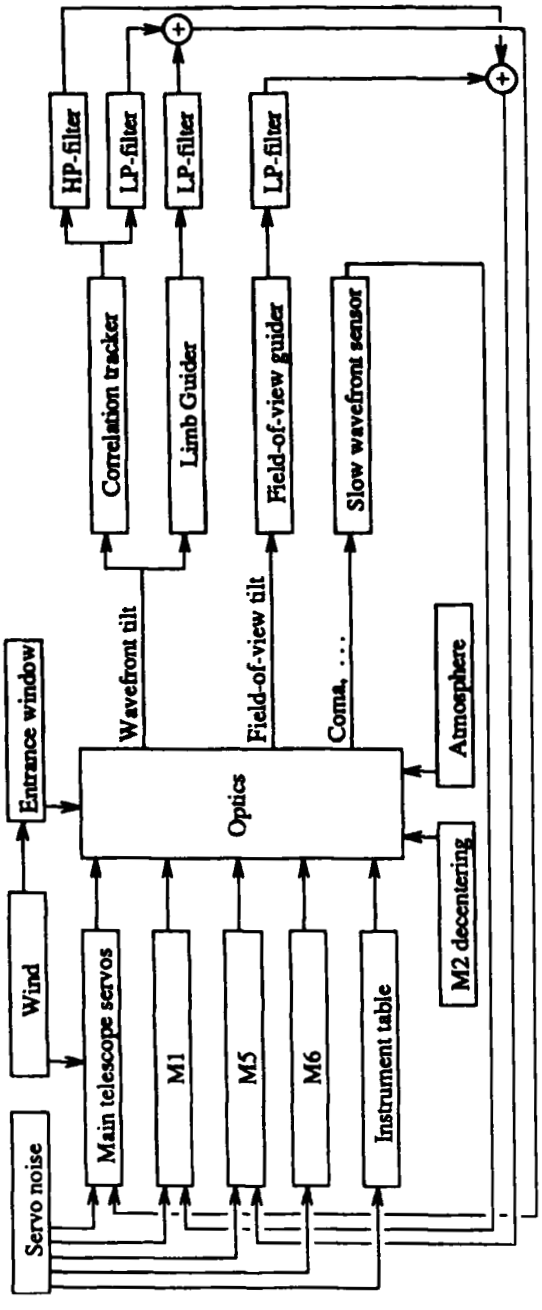

Figure 2 Overview of the LEST live optics system.

A model of the LEST has to consist of many parts, or subsystems, as indicated by Figures 1 and 2. Also, many of the blocks seen in Figure 2 contain servo systems, some of which are part of the live optics system. Further, the live optics system itself consists of a number of "detectors": the correlation tracker, the limb guider, the field-of-view guider and the slow wavefront sensor. Finally, there are different kinds of disturbances which will affect the image quality of the telescope, such as atmospherically induced distortion of the wavefronts, wind gusts, servo noise, thermal effects and gravity.

Since the main purpose is to investigate the dynamical behaviour of the telescope over rather short periods of time, a few of the subsystems of the real telescope can be excluded from the model: their effects on the performance of the telescope can be shown to be almost entirely stationary, and thus not of any significant importance, during the time-scales investigated here. The vast majority of the subsystems of the telescope will, however, have to be included in the model. A more detailed review of the various subsystems of the telescope model is given in Jakobsson (1995).

4 MODEL OF IMAGE DEGRADING EFFECTS

The most severe kind of image degrading disturbance is likely to be the atmospherically induced distortion of the incoming wavefronts. Therefore, the modelling of that is described in some detail here.

4.1 Theory of Atmospheric Turbulence

A statistical description of phase fluctuations caused by atmospheric turbulence is given by the phase structure function D_ϕ. Provided that the medium, in this case the atmosphere, is locally homogeneous and locally isotropic, and that the turbulence is incompressible, the phase structure function can be defined as

$$D_\phi(\mathbf{r}) = \langle [\phi(\mathbf{r}' + \mathbf{r}) - \phi(\mathbf{r}')]^2 \rangle, \tag{1}$$

where "$\langle\ \rangle$" stands for an ensemble average. For values of $|\mathbf{r}|$ within the inertial subrange, i.e. larger than the size l_0 (the inner scale) below which viscous dissipation becomes important and smaller than the size L_0 (the outer scale) above which the assumption of isotropy is no longer valid, the turbulence obeys Kolmogorov statistics, and the phase structure function can be written as (Fried, 1965)

$$D_\phi = 6.88 \left(\frac{|\mathbf{r}|}{r_0} \right)^{5/3}, \tag{2}$$

where r_0 is Fried's parameter.

4.2 Generation of Stationary Wavefronts

There are several different methods for generation of simulations of stationary, atmospherically distorted wavefronts. McGlamery (1976) introduced a method working in the Fourier domain, where a matrix of complex, Gaussian random numbers was filtered through multiplication with the Kolmogorov spectrum. The result was then subjected to an inverse two-dimensional Fourier transform. This method is straightforward, but has the disadvantage that the energy content of the lowest spatial frequencies is not correctly modelled, due to the limited sampling of the Fourier transform as these spatial frequencies.

A way to avoid the problems with the modelling of the low spatial frequencies was introduced by Roddier (1990). His method does not involve any Fourier transforms. Instead, a random set of Zernike coefficients is generated. However, since the Zernike coefficients are not statistically independent, a set of random Karhunen–Loève coefficients (which *are* statistically independent) is first generated, and then converted to Zernike coefficients. Subsequently, the wavefront is computed by adding all the Zernike terms at each sampling point.

A problem with this method is that the maximum radial order n of the Zernike polynomials needed is roughly proportional to the highest spatial frequency one wishes to model correctly. The number of Zernike polynomials needed to calculate the phase at each point of the wavefront, if polynomials up to radial order n are used, is approximately proportional to n^2. This means problems with long computation times and possibly accumulation of numerical round-off errors if one wishes to include very high spatial frequencies. This is usually not a severe problem for the generation of a stationary wavefront the size of the telescope aperture. However, if this method is used for production of time series of wavefronts, for which an initial wavefront considerably larger than the telescope aperture is needed (see below), the method can be used only for generation of fairly short time series.

4.3 Generation of Time Series of Wavefronts

The basic idea for the generation of time series of atmospherically disorted wavefronts is to generate a large, stationary wavefront, and then blow it past the telescope aperture at some velocity v. This is in accordance with Taylor's hypothesis, for which the turbulence pattern of an atmospheric turbulence layer is assumed to blow past the observer faster than the pattern changes ("frozen turbulence").

Here, the comparatively simple method by McGlamery (1976) is used to generate stationary wavefronts, in spite of its somewhat dubious behaviour at low spatial frequencies. This turns out not to be a severe problem when generating time series of wavefronts. Since only a small part of the initial wavefront is used at each timestep, the lowest spatial frequencies of that wavefront are fairly well modelled. While it is well known that the phase structure function is not well modelled for the entire initial wavefront when generated this way, the deviations from theory are rather small for the individual wavefronts of the time series.

Through the use of Taylor's hypothesis, low spatial frequencies (whose theoretical characteristics are somewhat unclear in the first place, as seen below) will correspond to low temporal frequencies. Deviations from theoretical temporal behaviour might therefore occur at low frequencies. For some applications, however, such as this analysis of the dynamical behaviour of the LEST, with emphasis on relatively high frequencies, this is not a problem.

It should be noted that the behaviour of the wavefront at low spatial frequencies depends on the size of the outer scale L_0, the latter being the cause of some controversy. Widely varying values have been reported in the literature, ranging from only a few meters to several kilometers. Apart from the Kolmogorov spectrum, there are also alternative models of the power spectrum of the turbulence, taking a finite outer scale into account. The most well-known such model is probably the Von Karman spectrum (Tatarskii, 1961).

4.4 Generation of Longer Time Series

The maximum length of a time series is limited by the size of the initial wavefront and by the wind speed. The size of the former is, in turn, limited by computational resources. If the method introduced by McGlamery (1976) is used to generate the initial wavefront, a way to get around this limitation is to generate a rectangular wavefront, making it longer in the wind direction. The drawback is that the lowest sampling frequencies are different in the wind direction and perpendicular to it.

An alternative way to get longer time series would be to repeat the original time series several times. For time series produced using the method by Roddier (1990), this is not possible, since the original time series will not be periodic. Attempts to alternately use a mirror version of the original time series will also fail. Either the gradient of the phase in the wind direction will be discontinuous, or, if that is compensated for, artificial magnification of the phase gradient perpendicular to the wind direction will be introduced (Jakobsson, 1994). If a method producing periodic wavefronts has been used to generate the original wavefront, the repetition approach is possible. However, the periodicity of the long time series will introduce spikes of significant magnitude in the temporal power spectra of the wavefront aberrations, already after a few repetitions.

4.5 Combining Several Turbulence Layers

So far, the atmosphere has been modelled as if it consisted of only one turbulence layer. A multi-layer atmospheric model can be constructed through the addition of several one-layer models, where the phase ϕ_k of layer k contributes to the final wavefront ϕ according to its weight c_k, i.e.

$$\phi = \sum_k c_k \phi_k, \tag{3}$$

with the weights being scaled such that

$$\sum_k c_k^2 = 1. \tag{4}$$

Since, according to theory, the phase is proportional to $r_0^{-5/6}$, setting the weights is equivalent to setting different values of r_0 for different turbulence layers.

It has been found from experiment by Roddier *et al.* (1993) that only a few atmospheric turbulence layers contribute significantly to the distortion of the wavefront, at least during favourable seeing conditions at a good observatory site. Thus, a multi-layer model can be made fairly easily using a few one-layer models.

4.6 Other Image Degrading Effects

Apart from atmospheric turbulence, there are many other image degrading effects. Wind gusts affect the pointing and tracking of the telescope, and may possibly give rise to vibrations in the telescope structure. The servo systems of various subsystems of the telescope will experience some amount of servo noise, mostly caused by discretization of the encoders used. There will also be errors in the signals from the various detectors of the live optics system. For all but the signal from the correlation tracker to M5, these signals are low-pass filtered, which strongly reduces the influence of the noise. A more detailed description of the modelling of these image degrading effects can be found in Jakobsson (1995).

Finally, there are also some image degrading effects which vary very slowly, such as thermal effects, gravitational effects and variations of the helium pressure in the telescope tube. During the time-scales that are investigated here, these effects can be regarded as stationary.

5 MODEL TESTING AND SIMULATION RESULTS

5.1 Verification of Atmospheric Model

In order to analyse the time series of the atmospherically distorted wavefronts, the aberration coefficients of the Zernike polynomials are calculated. The Zernike polynomials form a complete, orthogonal set over the unit circle. Using the normalization suggested by Noll (1976), the amount a_k of a certain Zernike aberration Z_k present in a wavefront of radius R, given by its phase ϕ, is

$$a_k = \int Z_k(\mathbf{r})\phi(R\mathbf{r})w d^2\mathbf{r}, \tag{5}$$

where $w = 1/\pi$ and the integration is performed over the unit circle. This way, the amount of various Zernike aberrations is calculated for the wavefront at each time-step of the simulation, thus producing time series of the aberration coefficients.

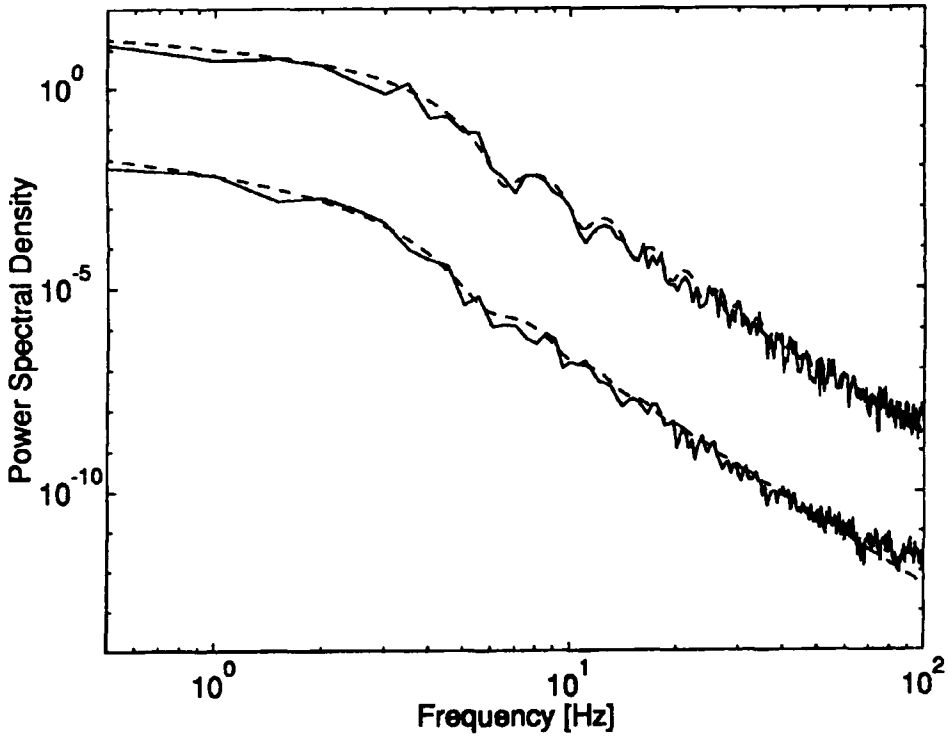

Figure 3 Mean power spectrum for 10 simulated time series of atmospherically distorted wavefronts (solid lines) compared to theoretical predictions (dashed lines). Zernike polynomial 2, x-tilt (upper curves) and 3, y-tilt (lower curves; vertically shifted).

In Figure 3, power spectra of Zernike coefficients 2 and 3 (tilts) are shown. The average of power spectra from ten different simulations is shown, reducing the amount of randomness in the curves. The simulation time was 2 s, the wind speed v was set to 10 m s^{-1} along the x-axis, the separation between grid points in both the x and y directions was 4 cm, and the telescope diameter was 2.4 m, equal to the diameter of the LEST. For convenience, power spectra of both Zernike coefficients are shown in the same figure. For clarity, the lower curves have been shifted downwards by a factor of 10^3, and the unit of the power spectral density is therefore arbitrary.

The temporal power spectra of the Zernike coefficients have been theoretically calculated by Conan *et al.* (1993), and by Roddier *et al.* (1993). The temporal power spectrum is found to have a low-frequency asymptote, which is different for different coefficients, and a high-frequency asymptote $\propto \nu^{-17/3}$ for all Zernike coefficients. The transition between low- and high-frequency behaviour is located at a cut-off frequency ν_c, which is found to be approximately (Conan *et al.*, 1993)

$$\nu_c = 0.3(n+1)v/D, \tag{6}$$

where D is the diameter of the telescope aperture.

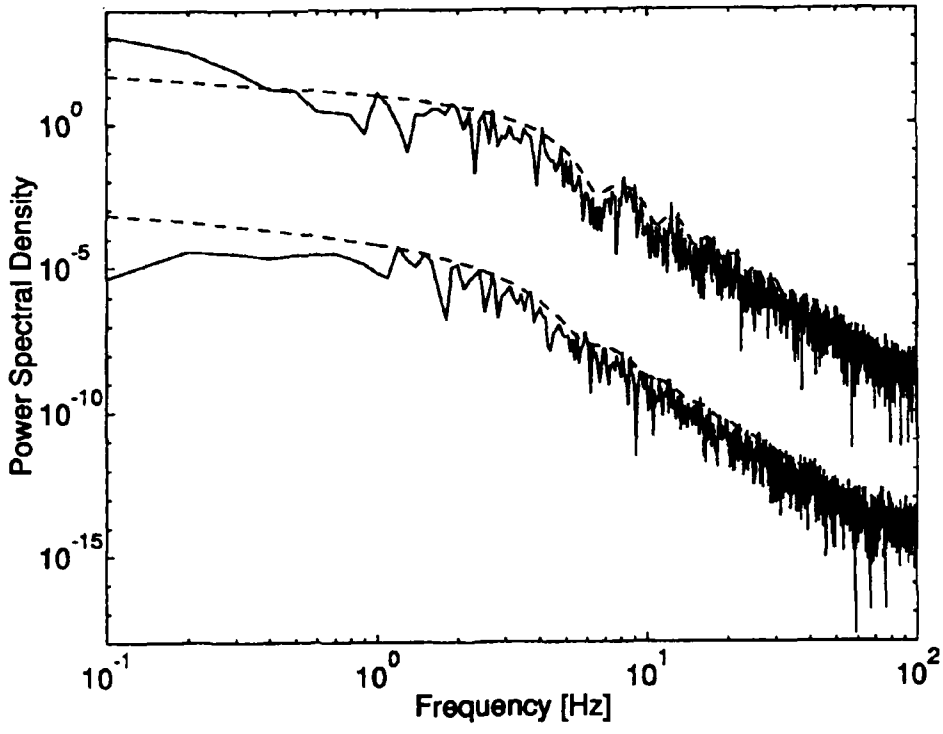

Figure 4 Power spectrum for a longer simulated time series of atmospherically distorted wavefronts (solid lines) compared to theoretical predictions (dashed lines). Zernike polynomial 2, x-tilt (upper curves) and 3, y-tilt (lower curves; vertically shifted).

The theoretical power spectra are shown as dashed lines. As seen in the figures, the agreement between theory and simulations is very good. The high-frequency parts closely follow the $\nu^{-17/3}$ dependence predicted (Conan *et al.*, 1993; Roddier *et al.*, 1993). Also, the low-frequency dependence seems to agree with theoretical predictions, although there are rather few data points at the lowest frequencies of the power spectra, making such a statement less certain. The cut-off frequencies ν_c also agree well with theory (Conan *et al.*, 1993) and experimental results (Madec *et al.*, 1992). The agreement is equally good for other Zernike aberrations.

The method for generation of longer time series was also tested. Power spectra from a simulation for which the size of the initial wavefront was twice the telescope diameter in the direction perpendicular to the wind direction and considerably larger in the wind direction are seen in Figure 4. Here, the lower curves in the figure have been shifted downwards by a factor of 10^5. The simulation time was 10 s, while grid point spacing, wind speed, wind direction and telescope diameter were the same as above. The high- and intermediate frequency parts of the power spectra still agree very well with theory, as do the positions of ν_c. At low frequencies, however, some noticeable deviation from theory is seen, reflecting the inaccurate modelling of the

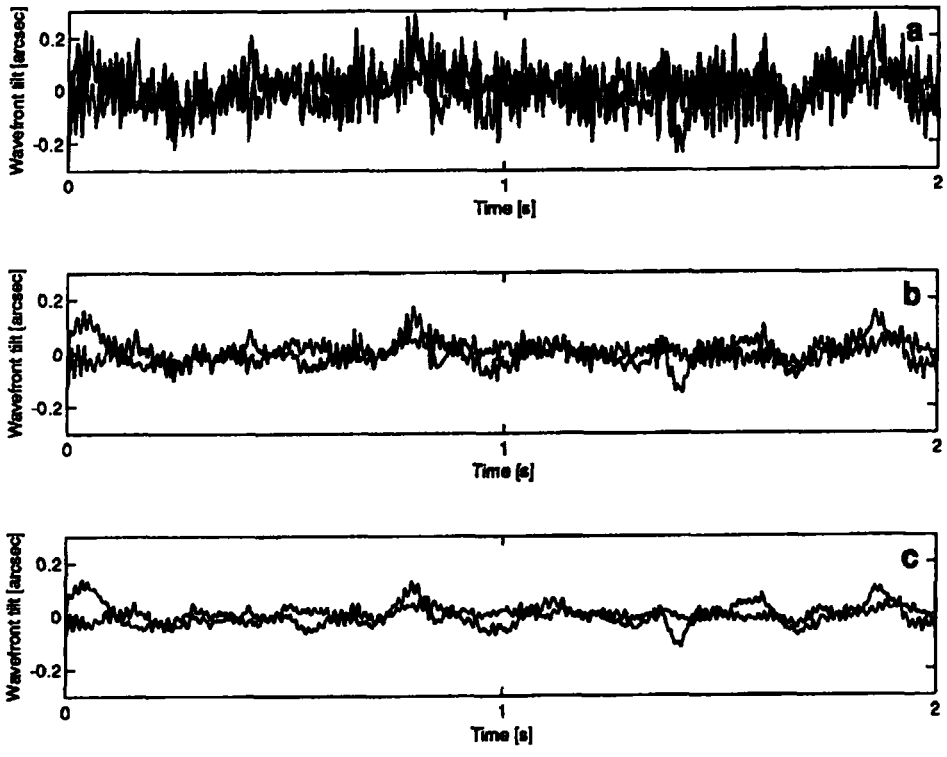

Figure 5 Simulation results with all noise sources included. *a*, Poor seeing (r_0 = 7.5 cm); *b*, good seeing (r_0 = 15 cm); *c*, excellent seeing (r_0 = 30 cm). All other parameters were the same during all three simulations.

lowest spatial frequencies in the direction perpendicular to the wind. While the overall randomness of the curves is the same for the individual power spectra used to produce Figure 3, no data points in these individual spectra differ as much from the theoretical curve, as some are seen to do at low frequencies in Figure 4.

5.2 Atmospheric Influence on Telescope Performance

In the final simulations, all image degrading sources are included. The one that is most critical to the image quality is the atmospheric turbulence. Figure 5 shows an example of simulations, where the effects of atmospheric turbulence can be seen clearly. Three different cases are shown, with the seeing being poor, good and excellent, respectively. In the figure, the values of r_0 were set to 7.5 cm (poor seeing), 15 cm (good) and 30 cm (excellent), respectively.

The atmosphere consisted of three different turbulence layers: One high altitude layer, where the wind speed v was set to 50 m s^{-1}, one boundary layer (v = 10 m s^{-1}) and one surface layer, with v = 10 m s^{-1}. The total effect of the

atmospheric turbulence is found by superimposing the different layers, using different weights for each layer. The weights of the different layers, scaled so that the sum of the squares of the weights equals one, were set to $1/\sqrt{6}$, $2/\sqrt{6}$ and $1/\sqrt{6}$, respectively.

As seen from the figure, the atmospheric turbulence has a very significant influence on the image motion in the final focus F3, especially when one compares the cases of poor and good seeing. The difference between good and excellent seeing is not as large, since the relative contribution of the atmospheric turbulence to the image quality is smaller. Instead, other effects, most notably servo noise and wind gusts, limit the improvement of the image quality.

Acknowledgements

T. Andersen, A. Ardeberg and O. Engvold are acknowledged for their help and support during the planning and implementation of this model.

References

Andersen, T., Engvold, O., and Jakobsson, H. (1993) In *Proc. 13th Sacramento Peak Workshop on Real Time and Post Facto Solar Image Correction*, R. R. Radick (ed.), Sunspot, New Mexico, USA, p. 53.

Conan, J.-M., Madec, P.-Y., and Rousset, G. (1993) In *Proc. 13th Sacramento Peak Workshop on Real Time and Post Facto Solar Image Correction*, R. R. Radick (ed.), Sunspot, New Mexico, USA, p. 6.

Engvold, O. and Andersen, T. (eds.) (1990) *Status of the design of the Large Earth-based Solar Telescope* (LEST Foundation).

Fried, D. L. (1965) *J. Opt. Soc. Am.* **55**, 1427.

Jakobsson, H. (1994) In *Proc. Soc. Photo-opt. Instrum. Eng.*, F. Merkle and M. A. Ealey (eds.) **2201**, 314.

Jakobsson, H. (1995) In *Proc. Soc. Photo-opt. Instrum. Eng.*, P. T. Wallace (ed.) **2479**, 266.

Madec, P.-Y., Conan, J.-M. and Rousset, G. (1992) In *Proc. ESO conf. 42 on Progress in Telescope and Instrumentation Technologies*, M.-H. Ulrich (ed.), Garching, Germany, p. 471.

McGlamery, B. L. (1976) In *Proc. Soc. Photo-opt. Instrum. Eng.*, J. C. Urbach (ed.) **74**, 225.

Noll, R. J. (1976) *J. Opt. Soc. Am.* **66**, 207.

Roddier, F., Northcott, M. J., Graves, J. E., McKenna, D. L., and Roddier, D. (1993) *J. Opt. Soc. Am.* **A10**, 957.

Roddier, N. (1990) *Opt. Eng.* **29**, 1174.

Tatarskii, V. I. (1961) *Wave propagation in a turbulent medium*, McGraw-Hill, New York.